

# マテリアル先端リサーチインフラ利用報告書

## ARIM User's Report

[Release : 2023.07.28] [Update : 2023.05.25]

### 課題データ / Project Data

課題番号 Project Issue Number	22TU0108
利用課題名 Title	粒子照射によるSiC繊維の微細組織変化
利用した実施機関 Support Institute	東北大学 / Tohoku Univ.
機関外・機関内の利用 External or Internal Use	内部利用 (ARIM事業参画者以外) / Internal Use (by non ARIM members)
ARIM半導体基盤PF 関連課題 Related to ARIM-SETI	指定なし / No Designation
横断技術領域 Cross-Technology Area	計測・分析/Advanced Characterization
重要技術領域 Important Technology Area	高度なデバイス機能の発現を可能とするマテリアル/Materials allowing high-level device functions to be performed
キーワード Keywords	炭化物系セラミックス, 繊維分散型複合材料, 電子顕微鏡/Electron microscopy, 電子回折/Electron diffraction, セラミックスデバイス/ Ceramic device

### 利用者と利用形態 / User and Support Type

利用者名 (課題申請者) User Name (Project Applicant)	袁 欣偉
所属名 Affiliation	東北大学 金属材料研究所
共同利用者氏名 Names of Collaborators Excluding Supporters in the Hub and Spoke Institutes	
ARIM実施機関支援担当者 Names of Supporters in the Hub and Spoke Institutes	
利用形態 Support Type	技術代行/Technology Substitution

### 利用した主な設備 / Equipment Used in This Project

利用した主な設備 Equipment ID & Name	TU-504 : 超高分解能透過電子顕微鏡
---------------------------------	-----------------------

## 報告書データ / Report

<p><b>概要 (目的・用途・実施内容)</b>  <b>Abstract (Aim, Use Applications and Contents)</b></p>	<p>SiCf/SiC composites, due to low radio activation, were considered one of the candidates for the blankets for the fusion reactors. The composite strength are closely related to the fiber microstructure changes. Past research showed that the Hi Nicalon TypeS (HNLS) fiber shrined after the irradiation at 300°C. The mechanism of the irradiation-induced fiber shrinkage is not clear. This work aims to clarify the relation between fiber shrinkage and irradiation temperature. SiCf/SiC were irradiated to ~100dpa with Si<sup>2+</sup> ion. The experimental temperature was kept at 30°C. Results show that fibers did not shrine after irradiation but show the amorphization of fibers.</p>
<p><b>実験</b>  <b>Experimental</b></p>	<p>The SiC<sub>f</sub>/SiC composites were unidirectionally reinforced with HNLS (NGS Advanced Fibers Co., Ltd., Toyama, Japan) and TSA3 (Ube Industries, Ltd., Ube, Japan) fibers. The SiC fiber surfaces were primarily coated with a thick (50–150 nm) layer of pyrolytic carbon (PyC). Subsequently, a PyC/SiC multilayered interface was created between the fiber and matrix. This is because the multilayered interface (ML) is well selected in fiber-reinforced composites to improve the crack resistance (e.g., crack deflection) and protect against environmental attacks (e.g., oxidation-induced resumption of PyC) in engineering. The ML interface consisted of five permutations of approximately 20-nm-thick PyC layer and 100-nm-thick SiC layer five times using the chemical vapor infiltration (CVI) method. The SiC matrix was created on the thin PyC layer of ML furthest from the fiber center using the CVI method (CVIed-SiC). To investigate the properties of the SiC fiber, SiCf/SiC was sliced perpendicular to the fiber axis. The sliced surface was polished to a mirror-like finish using diamond abrasive paper. The superior flatness and finish of the polished fiber surface were ensured using an optical microscope. The polished surface was settled to the water-cooling stage of the accelerator to maintain the temperature of the specimens under irradiation close to 30 °C. The surface temperature of the specimen was monitored during the entire irradiation test. The direction of the polished surface was perpendicular to the ion beam incidence. Both the SiCf/SiC composites reinforced by HNLS and TSA3 were exposed to a 5.1-MeV Si<sup>2+</sup> ion beam to an average damage level of over 100 dpa at the Dual-beam Irradiation Facility (DuET) at Kyoto University. To clarify the microstructural changes of the fibers, thin foils of both irradiated fibers were fabricated using the dual-beam FEI Helios NanoLab (FEI, Hillsboro, United States). The foils were examined using a scanning TEM (STEM; JEM-ARM200F, JEOL Ltd., Tokyo, Japan) at 200 kV.</p>

結果と考察  
Results and Discussion

To study the different irradiation behaviors of HNLS, TSA3, and CVled-SiC, microscopic observations of both SiC<sub>f</sub>/SiC specimens were performed by SEM & STEM under the bright field mode (BF), as depicted in Figs. 1 and 2, respectively. The morphologies of the fibers are shown in Figs. 1a and 2a. The selected fiber shape is circular if observed along the incident direction of the ion beam. The approximate observed region is boxed with a yellow frame. The incidence direction of the Si ion beam is from the top of Figs. 1b and 2b to the bottom. The microstructures of both the HNLS fiber and the ML interface are shown in Fig. 1. Because the axis of most fibers was initially perpendicular to the polished surface, we can consider that the radial tilt of the fibers parallel to the surface of the thin foil in Fig. 1b was induced by irradiation. A boundary exists at the depth of the surface, as shown in Fig. 1b. This is caused by the limited depth of the effects of silicon ion beam irradiation (the maximum irradiation depth for the Si ion beam in SiC is approximately 2.3 μm). It is the boundary between the irradiated and unirradiated areas. A clear difference in crystallinity was observed between the irradiated and unirradiated areas. Nanograins were easily observed at the unirradiated site. However, the microstructure of the irradiated area looked like a “sea.” Selected-area electron diffraction (SAED) was used to identify the crystallinity of both regions; the SAED patterns are shown in Fig. 1c. The variation from the polycrystalline pattern (unirradiated area) to the amorphous pattern (irradiated area) indicated that HNLS completely amorphized from the surface after the irradiation at 30 °C. Although the damage estimation for the surface is inaccurate, complete amorphization strongly implies that the amorphization of HNLS may start at a damage lower than 35 dpa (damage at the surface). In summary, the microstructure of HNLS exhibited an amorphous (irradiated) to polycrystalline (unirradiated) structure with depth. For the ML interface, the transformation of crystallinity from polycrystalline to amorphization was also observed. In addition, the polycrystalline area was maintained close to the surface. The SAED pattern shown in Fig. 1c-4 reveals polycrystalline rings. The polycrystalline area is marked by a blue frame and enlarged in Fig. 1b. The width of the polycrystalline band was approximately 660 nm starting from the surface. The amount of irradiation damage at a depth of 660 nm corresponds to approximately 70 dpa. Thus, the observed area of the ML interface showed the following microstructure according to depth: polycrystalline (low-dose)–amorphous (high-dose)–polycrystalline (unirradiated). Microstructural observations of the TSA3 fiber, ML, and matrix under the BF mode and low-angle annular dark-field (LAADF) mode are shown in Fig. 2b. The TSA3 fiber showed a microstructure with different crystallinities according to depth: polycrystalline–amorphous–polycrystalline (corresponding to low-dose to high-dose to unirradiated), as shown in Fig. 2b. The polycrystalline area was enlarged and further observed in the LAADF mode, as shown in Figs. 2c and 2d. A transformation from polycrystalline to amorphous was also detected from this band via SAED, as depicted in Figs. 2g-1 and 2g-2. The depth of the polycrystalline band was approximately 450 nm. The amount of irradiation damage at 450 nm was approximately 60 dpa. An arc-shaped region, indicated with the black arrow, was observed, as shown in Fig. 2b. This may be one of the PyC layers coated on the fiber. The unirradiated region of the TSA3 fiber was not observed in the thin foil. For the interface, the ML in the TSA3 fiber-reinforced SiC<sub>f</sub>/SiC shows a semi-elliptical shape that differs from that of the ML interface nearly parallel to the HNLS axis which is observed in the cross-sectional surface shown in Fig. 1b. The change in the profile of the ML interface on the cross-section from parallel straight lines (Fig. 1b) to a semi-elliptical shape implies a tilt of the ML interface and TSA3 toward the direction of incidence of the observed electron beam. In this case, the ML interface, which was initially perpendicular to the fiber axis, exhibited a semi-elliptical shape. For the CVled matrix, the polycrystalline–amorphous–polycrystalline structure was observed by both microstructural observation and SAED patterns, as shown in Fig. 2c. The width of the polycrystalline band in the matrix was approximately 550 nm. The electron diffraction analysis was performed at each part of the polycrystalline–amorphous–polycrystalline structure of the matrix using a selected-area aperture of the same size; the SAED patterns are shown in Fig. 2g. The unirradiated matrix shows a polycrystalline diffraction pattern (Fig. 5g-5). Moreover, the polycrystalline rings in the diffraction pattern of the polycrystalline area close to the surface (Fig. 2g-6) become darker and sparser than the unirradiated ones (Fig. 2g-5). As the depth from the incident surface or the irradiation damage increased, the diffraction pattern was completely transformed from polycrystalline (Fig. 2g-6) to amorphous (Fig. 2g-7). Furthermore, morphological changes were observed in the grain boundaries of TSA3 and CVled-SiC after irradiation. A conspicuous amorphous phase appeared along the possibly original grain boundaries in the TSA3 and the CVled-SiC, as indicated by the yellow arrows in Figs. 2d and 2f. A similar phase was not observed in the samples from the same lot but irradiated at higher irradiation temperatures.

図・表・数式 1  
 Figures, Tables and  
 Equations 1

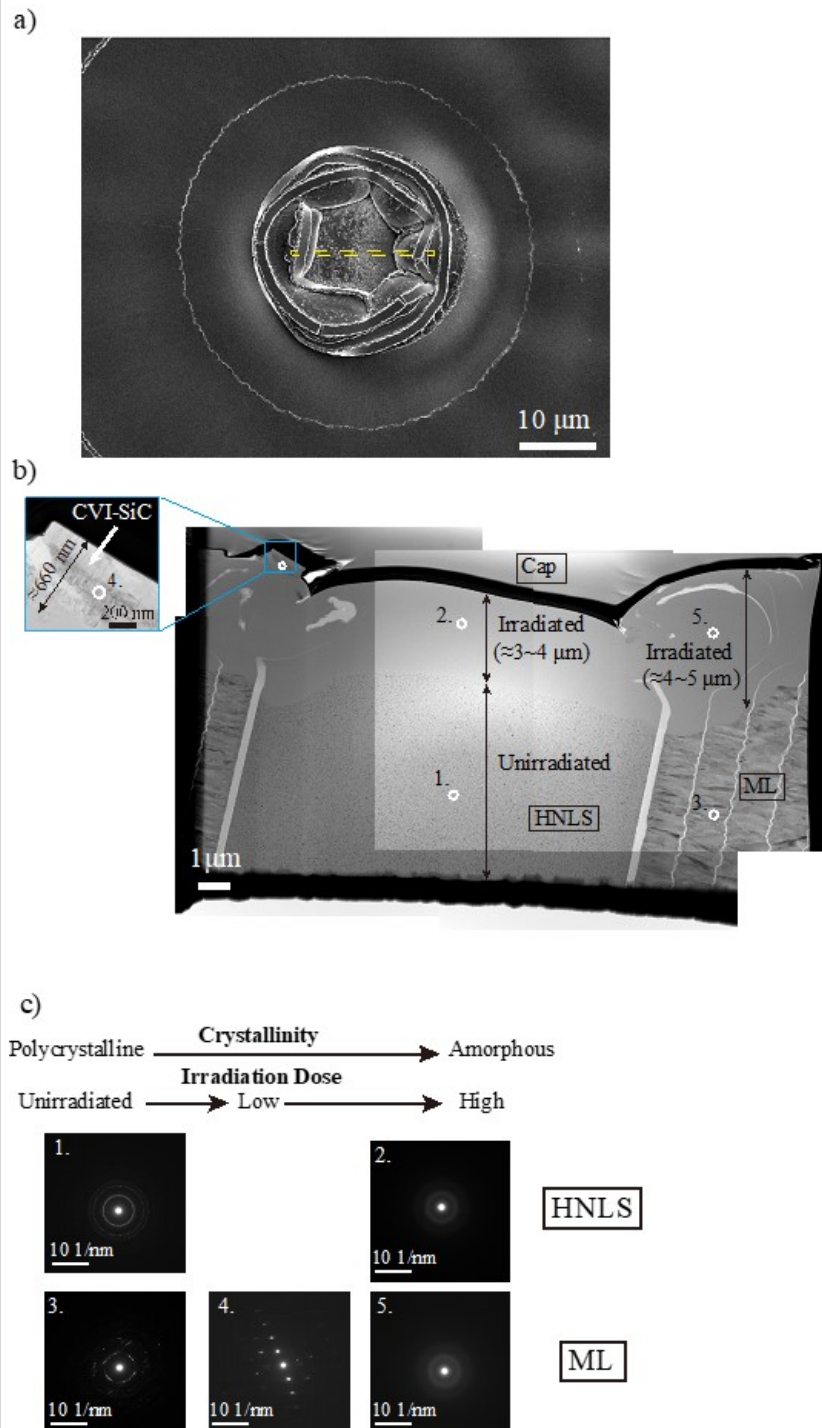


Fig. 1 Morphology of selected HNLS fiber for microstructural observation. (a) Surface morphology for observed HNLS fibers. (b) Microstructure of HNLS fiber-reinforced  $\text{SiC}_f/\text{SiC}$  composite under room-temperature irradiation. (c) Electron diffraction pattern of circled area in (b). The yellow frame in (a) is the approximate region observed in (b).

<p>図・表・数式 2 Figures, Tables and Equations 2</p>	<p>Fig.2 Morphology of selected TSA3 fiber from microstructural observation. (a) Surface morphology of observed TSA3 fiber. (c) Enlarged morphology of area in (b) circled with a blue frame. (d) Enlarged morphology of area in (c) circled with a green frame. (e) Enlarged morphology of area in (b) circled with a yellow frame. (f) Enlarged morphology of area in (c) circled with a purple frame. (g) Electron diffraction pattern of circled area in (b) to (f). Note that the yellow frame in (a) is the approximate observed region for (b).</p>
<p>その他・特記事項 (参考文献・謝辞等) Remarks(References and Acknowledgements)</p>	<p>This work was performed under the GIMRT Program of the Institute for Materials Research, Tohoku University (proposal number 202012 CRKEQ 0418) and the Joint Usage/Research Program on Zero-Emission Energy Research, Institute of Advanced Energy, Kyoto University (proposal number ZE2022A-04) and financially supported by JST SPRING (grant number JPMJSP2114) and technically supported by Material Solutions Center (MaSC), Tohoku University, Japan.</p>

### 成果発表・成果利用 / Publication and Patents

<p>DOI (論文・プロシーディング) DOI (Publication and Proceedings)</p>	
<p>口頭発表、ポスター発表 および、その他の論文 Oral Presentations etc.</p>	
<p>特許出願件数 Number of Patent Applications</p>	0件
<p>特許登録件数 Number of Registered Patents</p>	0件